ACS APPLIED ELECTRONIC MATERIALS

pubs.acs.org/acsaelm Article

Unraveling the Ultrafast Self-assembly and Photoluminescence in Zero-Dimensional Mn^{2+}-Based Halides with Narrow-Band Green Emissions

Guojun Zhou,[▽] Qiqiong Ren,[▽] Maxim S. Molokeev, Yayun Zhou, Jian Zhang,* and Xian-Ming Zhang*

Cite This: *ACS Appl. Electron. Mater.* 2021, 3, 4144−4150 Read Online

ACCESS | Metrics & More | Article Recommendations | Supporting Information

ABSTRACT: The discovery of narrow-band luminescent materials remains an immense challenge to optimize the performance of white light-emitting diodes (LEDs). So far, the zero-dimensional (0D) Mn^{2+}-based halides with near-unity narrow-band emissions have emerged as a class of promising phosphors in solid-state displays, but the related large-scale synthesis strategies have not been proposed and evaluated. Herein, we report an in situ synthetic process of 0D Mn^{2+}-based halides and utilize $(C_{20}H_{20}P)_2MnBr_4$ as a case to investigate the photoluminescence characteristics and the structural essence of ultrafast self-assembly. The bright green emission peak at 523 nm with a full width at half maximum of 48 nm for $(C_{20}H_{20}P)_2MnBr_4$ is attributed to the d−d transition ($^4T_1$−$^6A_1$) of tetrahedrally coordinated $[MnBr_4]^{2-}$ centers, and the fabricated white LED device shows a wide color gamut of 103.7% National Television System Committee (NTSC) standard. Remarkably, the experimental and theoretical results indicate that there are hydrogen bonding of C−H···Br and weak van der Waals interactions between $[C_{20}H_{20}P]^+$ and $[MnBr_4]^{2-}$, resulting in the root for the realization of ultrafast self-assembly in 0D Mn^{2+}-based halides. This work reveals a feasible and general synthesis method for preparing 0D Mn^{2+}-based halides, thereby providing a possibility for their industrial application in solid-state displays.

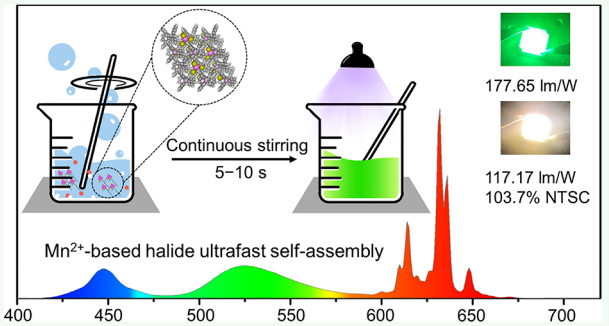

KEYWORDS: *zero-dimensional Mn^{2+}-based halides, ultrafast self-assembly, photoluminescence, white LEDs, solid-state displays*

INTRODUCTION

Finding narrow-band green-light emitters for application in solid-state displays is an immense and rewarding challenge.[1,2] Hybrid metal halides possess fascinating photoluminescence (PL) properties that can be tuned by regulating the structural dimensions and chemical components.[3−8] Among these, the zero-dimensional (0D) Mn^{2+}-based halides have emerged as a class of promising narrow-band phosphors due to their excellent green emission with a full width at half maximum (fwhm) of <60 nm and high photoluminescence quantum yields (PLQYs) of >80%.[9−12] Compared to the commercial rare-earth phosphor β-sialon:Eu^{2+},[13] the 0D Mn^{2+}-based halides exhibit a narrower green emission, which is conducive to improving the color gamut of white light-emitting diodes (LEDs) and suppressing the loss of strategic resource of europium. It should be noted that large-scale batch production methods are important for their further practical applications and the following should be considered: low energy consumption, low pollution, easy operation, and short growth cycle.[14,15]

A variety of 0D Mn^{2+}-based/Mn^{2+}-doped halides have been reported, resulting in green-light emissions and red-light emissions, respectively.[11,12,16−24] In this work, we emphasize and investigate the synthesis methods, crystal structure, and PL characteristics of 0D Mn^{2+}-based halides with narrow-band green emissions. It is worth noting that the halogen atoms and subtle changes in crystal structure will become factors in regulating the fluorescence emission peak position (500−550 nm), emission line widths (40−60 nm), and lifetimes (the shortest for iodides, the second for bromides, and the longest for chlorides) by influencing the ligand-field effects and nephelauxetic effects.[9,24] Moreover, Xia et al. and Seshadri et al. have discussed in depth the tuning relationship between the crystal structure and luminescence performances and found that a sufficiently long Mn···Mn distance enables all Mn^{2+} centers to emit spontaneously, thereby leading to near-unity narrow-band green-light emissions in 0D Mn^{2+}-based halides.[10,25] Even though most Mn^{2+}-based emitters were applied as green-light components in LCD backlight and similar 0D Mn^{2+}-based halides show a good application

Received: July 8, 2021
Accepted: August 19, 2021
Published: August 29, 2021

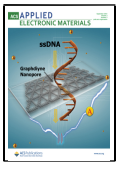

https://doi.org/10.1021/acsaelm.1c00606
ACS Appl. Electron. Mater. 2021, 3, 4144−4150

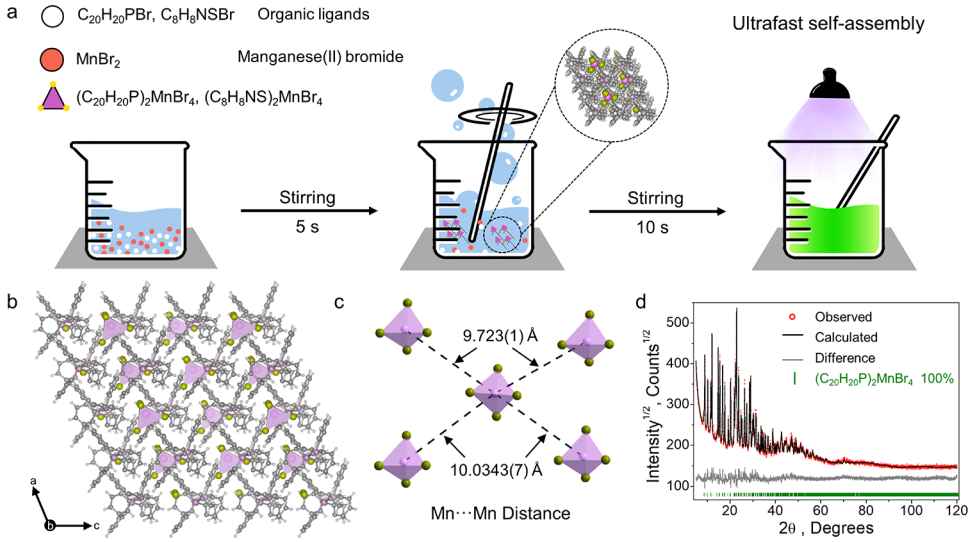

Figure 1. (a) Schematic illustration for the synthesis of $(C_{20}H_{20}P)_2MnBr_4$ and $(C_8H_8NS)_2MnBr_4$ through an ultrafast self-assembly process; the ultrafast self-assembly process refers to the rapid formation of the C−H···Br hydrogen bonds and the van der Waals interactions between organic ligands and inorganic building units. The inset is the single-crystal structure at the molecular level. (b) View of the single-crystal structure of $(C_{20}H_{20}P)_2MnBr_4$ (color scheme: $[MnBr_4]^{2-}$, purple tetrahedron; Mn, purple atoms; Br, yellow atoms; organic cations, gray atoms). (c) Diagram of the distance of two adjacent Mn^{2+} in a $[MnBr_4]^{2-}$ tetrahedron. (d) Difference Rietveld plot of the $(C_{20}H_{20}P)_2MnBr_4$ powder.

prospect in the field of solid-state displays, an easy-to-operate and large-scale synthesis method has not been proposed, and the characteristics of ultrafast self-assembly have not yet been fundamentally unraveled. It is well known that the preparation methods of metal halides are as follows: cooling crystallization, antisolvent crystallization, hydrothermal crystallization, etc. Most of 0D Mn^{2+}-based halides referring to single crystals and powders were prepared by the cooling crystallization method in acid solution or organic solvent (such as DMF, methanol, etc.), which not only resulted in a relatively long reaction cycle about a few hours or even days but also the discharge of acid waste liquid or organic liquid during the synthesis process.[26−28] Accordingly, it is extremely urgent to develop a synthetic strategy with easy operation, low cost, short cycle, and environment-friendliness to promote their practical application.

Herein, an ultrafast and easy-to-operate synthesis method is proposed: A series of narrow-band green-emitting 0D Mn^{2+}-based halides can be obtained by continuous stirring in ethanol solution at room temperature (RT) for 5−10 s, and these materials have aroused interest for application in solid-state displays. Based on theoretical and experimental results, $(C_{20}H_{20}P)_2MnBr_4$ as a case is used to reveal the structural origin of ultrafast self-assembly and photoluminescence characteristics. It is demonstrated that there widely exists the hydrogen bonding of C−H···Br interactions, in addition to weak van der Waals (vdW) attractive interactions between $[C_{20}H_{20}P]^+$ and $[MnBr_4]^{2-}$, which is the root cause for the realization of ultrafast self-assembly in 0D Mn^{2+}-based halides. In addition, $(C_{20}H_{20}P)_2MnBr_4$ exhibits a near-unity narrow-band green emission at 523 nm, and the fabricated white LED presents a high luminous efficacy of 117.17 lm/W and a wide color gamut of 103.7% National Television System Committee (NTSC) standard. This synthetic strategy of ultrafast self-assembly at RT aims at paving the way for the industrial application of 0D Mn^{2+}-based halides in solid-state displays.

EXPERIMENTAL SECTION

Materials and Preparation. $C_{20}H_{20}PBr$ (ethyltriphenylphosphonium bromide, 98%, Aladdin), C_8H_8NSBr (2-methylbenzothiazole hydrobromate), $MnBr_2{\cdot}4H_2O$ (98%, Aladdin), and CH_3CH_2OH (ethanol, 99.7%, Sinopharm) were used in this study. $MnBr_2{\cdot}4H_2O$ was dried at 120 °C for 6 h for later use, and other chemicals were used as received.

$(C_{20}H_{20}P)_2MnBr_4$ was prepared by dissolving $C_{20}H_{20}PBr$ (2 mmol) and $MnBr_2$ (1 mmol) in 5 mL of ethanol. The powder of $(C_{20}H_{20}P)_2MnBr_4$ could be obtained immediately at RT under slight stirring for about 5−10 s. When the temperature was raised to about 60 °C, a clear ethanol solution was obtained under continuous stirring. The single crystal of $(C_{20}H_{20}P)_2MnBr_4$ was synthesized by slow cooling from 60 °C to RT. As for $(C_8H_8NS)_2MnBr_4$, the synthesis method was consistent with the above method. The white LED was fabricated using $(C_{20}H_{20}P)_2MnBr_4$, K_2SiF_6:Mn^{4+} (KSF/Mn^{4+}), and a GaN LED chip (450 nm). These phosphors were first thoroughly mixed with epoxy resin, and then the above mixture was evenly coated on the surface of the blue chip to obtain the white LED device.

Characterization. Single-crystal X-ray diffraction was conducted on an Agilent Technologies Gemini EOS diffractometer with a Mo-Kα radiation source (λ = 0.71073 Å). Powder X-ray diffraction (PXRD) was performed on an Aeris powder diffractometer (PANalytical Corporation) operating at 40 kV and 15 mA with Cu-Kα radiation (λ = 1.5406 Å). The Rietveld refinement was performed using TOPAS 4.2. The photoluminescence excitation/emission (PLE/PL) spectra, PL decay curves, and photoluminescence quantum yields (PLQYs) were measured on a FLSP9200 fluorescence spectrophotometer (Edinburgh Instruments Ltd., U.K.) at RT. The temperature-dependent spectra were measured on a FLSP9200 fluorescence spectrophotometer with additional controllable heating equipment. The thermogravimetric analysis (TGA) was carried out on the SETARAM 131 LABSYS equipment at a heating rate of 10 °C/min from RT to 800 °C. The emission spectra, CIE coordinates, and luminous efficacy of LED devices were performed on an integrating sphere spectroradiometer system (ATA-100, Everfine).

Computational Methods. The quantum chemistry calculations were carried out using the Gaussian-09 software package and analyzed with Multiwfn software.[29] DFT calculations using the hybrid B3LYP were performed during the geometry optimization and estimation of the electron charge distribution process. The Mn and Br atoms were

https://doi.org/10.1021/acsaelm.1c00606
ACS Appl. Electron. Mater. 2021, 3, 4144−4150

treated using a LanL2DZ basis set, while for other atoms (P, C, and H), the standard Pople basis set 6-31G (d,p) was used.[30,31] The first-principles calculations were performed on the plane-wave formalism as implemented in the Vienna ab initio simulation package (VASP).[32] The Perdew–Burke–Ernzerhof (PBE) formulation was applied to describe the exchange–correlation under the generalized gradient approximation (GGA).[33] Plane-wave functions were expanded with an energy cutoff of 400 eV and Brillouin zone-sampled using a 1 × 2 × 2 gamma-centered κ-mesh. For electronic calculations, the Heyd–Scuseria–Ernzerhof (HSE06)[34] functional was used to provide a more accurate estimate.

RESULTS AND DISCUSSION

Zero-dimensional (0D) Mn^{2+}-based halides exhibit excellent PL properties, making them become the potential narrow-band emitters in solid-state displays. It is well known that almost all Mn^{2+}-based halides are synthesized in acid solution or organic solvent, and their growth cycle is within a few hours or even days.[9,27]

In this work, a brand-new synthesis method with the advantages of ultrafast reaction and easy operation is proposed for 0D Mn^{2+}-based halides, which is of great significance to the implementation of industrial applications. As shown in Figure 1a, a mixture of $C_{20}H_{20}PBr/C_8H_8NSBr$ and $MnBr_2$ at a molar ratio of 2:1 is dissolved in ethanol after continuous stirring for 5–10 s, and the suspension presents green fluorescence upon 365 nm UV light immediately. We consider that the reaction is an ultrafast self-assembly process, in which the organic ligand and inorganic polyhedron quickly form a complete crystal structure. To verify the feasibility and versatility of the ultrafast self-assembly, the Mn^{2+}-based halides $(C_{20}H_{20}P)_2MnBr_4$ and $(C_8H_8NS)_2MnBr_4$ are synthesized in ethanol solution under brief stirring, and they all present green fluorescence upon 365 nm UV light immediately. Moreover, the corresponding single crystals were prepared by the cooling crystallization method for the analysis of the phase and structure of products. Their crystallographic data are deposited in the Cambridge Crystallographic Data Centre (CCDC#2084475-2084476), and the main structure parameters are shown in Table 1 and Tables S1 and S2. As predicted, a typical 0D structure at the molecular level is obtained and displayed in Figure 1b and Figure S1a, which demonstrates that all Mn atom coordinates with four adjacent Br atoms form the $[MnBr_4]^{2-}$ tetrahedron, and the tetrahedron is spatially isolated by surrounding $[C_{20}H_{20}P]^+$/$[C_8H_8NS]^+$ organic cations. The CIE coordinates and digital photos (Figure S2) illustrate that they all present the green-light emission. In addition, the reported green-emitting 0D Mn^{2+}-based halides $(C_{24}H_{20}P)_2MnBr_4$ and $(C_{10}H_{16}N)_2MnBr_4$ can also be obtained by brief stirring in ethanol solution, which indicates that this synthesis strategy is feasible for most Mn^{2+}-based halides.

Table 1. Main Structure Parameters of $(C_{20}H_{20}P)_2MnBr_4$ and $(C_8H_8NS)_2MnBr_4$

compounds	$(C_{20}H_{20}P)_2MnBr_4$	$(C_8H_8NS)_2MnBr_4$
weight (g/mol)	951.19	674.97
space group (Z)	Cc, 4	P-1, 4
a (Å)	12.3309(10)	7.8618(3)
b (Å)	21.2999(14)	14.8011(7)
c (Å)	16.6036(16)	20.1414(9)
α (°)	90	77.014(4)
β (°)	111.515(10)	82.151(4)
γ (°)	90	75.874(4)
V (Å^3)	4057.0(6)	2206.42(18)
ρ_{calc} (g/cm^3)	1.557	2.032
$2\theta_{max}$ (°)	61.24	61.89
R_1 [$F_o > 4\sigma(F_o)$]	0.0583	0.0573
wR_2	0.1284	0.1406
Goof	0.993	0.935

On this basis, taking $(C_{20}H_{20}P)_2MnBr_4$ as a case, the structural origin of ultrafast self-assembly and PL characteristics of 0D Mn^{2+}-based halides are revealed in detail. As shown in Figure 1c, the large cations of $[C_{20}H_{20}P]^+$ have endowed a remote Mn···Mn distance, and the distances between two adjacent Mn^{2+} in a $[MnBr_4]^{2-}$ tetrahedron are 9.723 and 10.0343 Å, indicating that $(C_{20}H_{20}P)_2MnBr_4$ exhibits a strong PL emission with high PLQYs.[10,25] The PXRD data of $(C_{20}H_{20}P)_2MnBr_4$ for Rietveld analysis are refined using TOPAS 4.2, showing that all peaks are indexed by a monoclinic cell (Cc) with parameters close to single-crystal parameters. Refinement of profile parameters and cell parameters is stable with low R-factors (Figure 1d), which proves that the structure of the single crystal is representative of all bulk materials and the powder synthesized by ultrafast self-assembly is a single phase.

To gain insight into the intramolecular interactions in the compound $(C_{20}H_{20}P)_2MnBr_4$, the independent gradient model (IGM) analysis[35] was first implemented to illustrate the reaction active sites, interaction types, and interaction strengths and to explore the essence of the interactions between $[C_{20}H_{20}P]^+$ and $[MnBr_4]^{2-}$. To vividly show the interaction sites of different fragments, the colored map of the real space function $\mathrm{sign}(\lambda_2)\rho$, which means the sign of the second-largest eigenvalue of electron density Hessian matrix at position r, versus δ_g isosurfaces is drawn in the inset of Figure 2. The blue and green regions evidently correspond to the strong bond and weak vdW attractive interaction, respectively. As can be seen in the colored map, the hydrogen bond of C–H···Br is formed between $[C_{20}H_{20}P]^+$ and $[MnBr_4]^{2-}$, and there are some weak vdW interactions between different fragments. In the corresponding scatter diagram (Figure 2), there is a stronger peak located in the blue-green border, and there are some weaker peaks located in the green area, which are consistent with the results of the colored map analysis. It is almost certain that there widely exists weak vdW interactions in addition to the hydrogen bonding of C–H···Br interactions

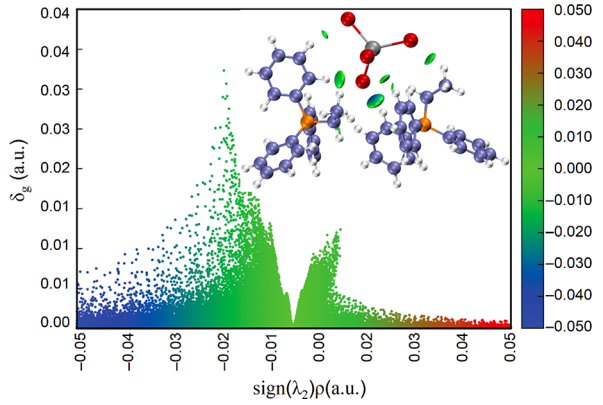

Figure 2. Scatter diagram of the δ_g isosurface versus $\mathrm{sign}(\lambda_2)\rho$ for the compound $(C_{20}H_{20}P)_2MnBr_4$ and the inset showing the corresponding scatter diagram of the δ_g isosurface versus $\mathrm{sign}(\lambda_2)\rho$.

https://doi.org/10.1021/acsaelm.1c00606
ACS Appl. Electron. Mater. 2021, 3, 4144–4150

between $[C_{20}H_{20}P]^+$ and $[MnBr_4]^{2-}$. These attractions can be the structural reason for the fast formation of the complex.

Table 2 summarizes the spin population and Mulliken charge of the Mn^{2+} ion for each spin multiplicity. The spin

Table 2. Spin Population and Mulliken Charge of a Mn^{2+} Ion for Each Spin Multiplicity

spin multiplicity	spin population	Mulliken charge (a.u.)	total energy (a.u.)
2	0.971	0.076	−2387.718
4	2.948	0.119	−2387.758
6	4.636	0.186	−2387.838

population is close to the number of lone pair electrons of Mn^{2+} ion (d^5) as expected. On the other side, the calculated Mulliken charges are from 0.076 to 0.186 for the Mn^{2+} ion because the charge of the metal ion is diminished by its delocalization over the complex. Based on the lowest total energy, the ground-state structures are obtained from the highest spin multiplicity (6). In addition, the Gibbs free energy change (ΔG) calculation was performed in an alcohol solvent using the solvation model based on density (SMD).[36] According to the formula $\Delta G = \sum G_{product} - \sum G_{reactant}$, it is found that the Gibbs free energy change of the reaction is −36.12 kcal/mol (Table 3), and this negative value of the

Table 3. Gibbs Free Energy Changes of the Products and Reactants of the Reaction

$G_{product}$ (kcal/mol)	$G_{reactant}$ (kcal/mol)	ΔG (kcal/mol)
−98,645.44	−98,609.32	−36.12

Gibbs free energy change in reaction process suggests that the chemical reaction can occur spontaneously and the reactants turn naturally into the product.

As shown in Figure 3a, the $(C_{20}H_{20}P)_2MnBr_4$ single crystal exhibits strong green fluorescence under an ultraviolet (UV) lamp of 365 nm. Meanwhile, it can be processed into different morphologies, including single crystal, powder, and thin film (Figure S3), indicating that such 0D emitters have relatively good machinability and flexibility. Their emission spectra and lifetimes are also consistent, so in the following, we focus on analyzing the PL characteristics of $(C_{20}H_{20}P)_2MnBr_4$ powder (Figure S4). As shown in Figure 3b, the excitation and emission spectra illustrate that $(C_{20}H_{20}P)_2MnBr_4$ shows a narrow-band green-light emission (fwhm = 48 nm, λ_{em} = 523 nm) ascribed to the $^4T_1-^6A_1$ transition of Mn^{2+} cation coordinated with four Br^- ions (Figure S5). From the excitation spectrum, $(C_{20}H_{20}P)_2MnBr_4$ can be excited by blue light (450 or 460 nm), which indicates that the corresponding white LED device possesses a great application prospect in solid-state displays. In Figure 3c, the PL decay curve at RT of $(C_{20}H_{20}P)_2MnBr_4$ excited at 365 nm and monitored at 523 nm is well fitted by the single exponential decay equation: $I(t) = I_0 + A \exp(-t/\tau)$, which indicates that $(C_{20}H_{20}P)_2MnBr_4$ has almost no radiation-free channels,[37] resulting in a relatively high PLQY of 93.83%, and the absorption efficiency is 28.76% under excitation at 450 nm (Figure S6). The lifetime is determined to be 0.312 ms, which is close to that of Mn^{2+}-based bromides reported so far.[9,11] Of course, the emission peak positions and lifetimes of $(C_{20}H_{20}P)_2MnBr_4$ measured under different excitations are consistent, as shown in Figure S7. To further reveal their optical properties, the band structure and densities of states (DOS) of $(C_{20}H_{20}P)_2MnBr_4$ were calculated by the HSE06 functional, as shown in Figure 4. The calculated HSE06 band gap is 2.57 eV, and it can be found that the valence band maximum (VBM) is mainly consisted of Br-p and Mn-d orbitals, while the conduction band minimum (CBM) is mainly contributed by the organic group $(C_{20}H_{20}P)$-p orbital. In addition, the sharp peaks near the VBM indicate that the valence band of $(C_{20}H_{20}P)_2MnBr_4$ is nearly dispersion-less, showing negligible electronic coupling between $[MnBr_4]^{2-}$ clusters.

Thermal quenching behavior is a key indicator to evaluate its application prospects in solid-state displays. Figure 3d presents

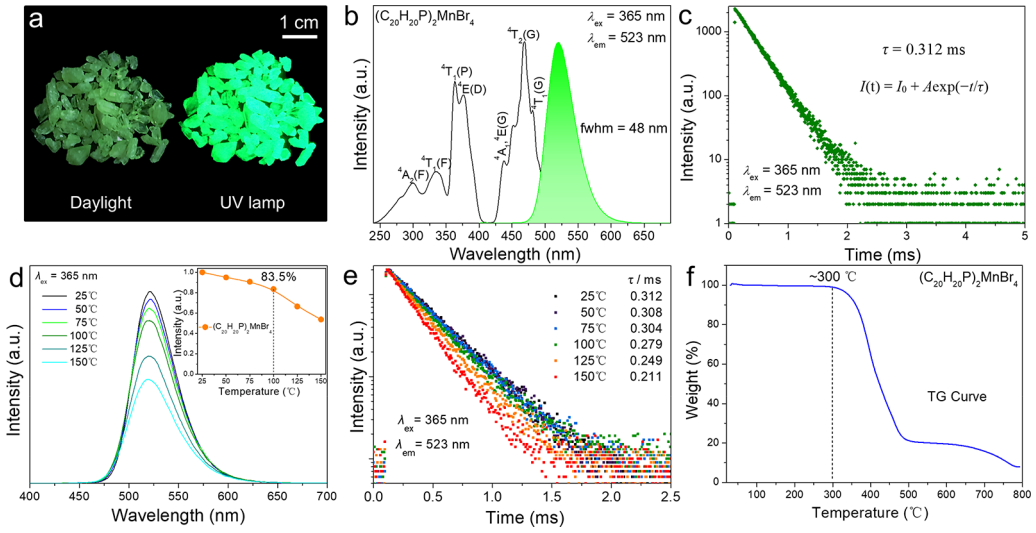

Figure 3. (a) Physical images of a $(C_{20}H_{20}P)_2MnBr_4$ single crystal under daylight and a UV lamp. (b) Photoluminescence excitation (black) and emission (green) spectra of $(C_{20}H_{20}P)_2MnBr_4$ at RT. (c) Luminescence decay curve of $(C_{20}H_{20}P)_2MnBr_4$ excited at 365 nm and monitored at 523 nm. (d) Temperature-dependent PL spectra of $(C_{20}H_{20}P)_2MnBr_4$ under excitation at 365 nm. A variable trend of integrated intensity with the increase in temperature is shown in the inset. (e) Temperature-dependent PL decay spectra of $(C_{20}H_{20}P)_2MnBr_4$ under excitation at 365 nm and monitored at 523 nm. (f) TGA curve for the powder sample of $(C_{20}H_{20}P)_2MnBr_4$.

https://doi.org/10.1021/acsaelm.1c00606
ACS Appl. Electron. Mater. 2021, 3, 4144−4150

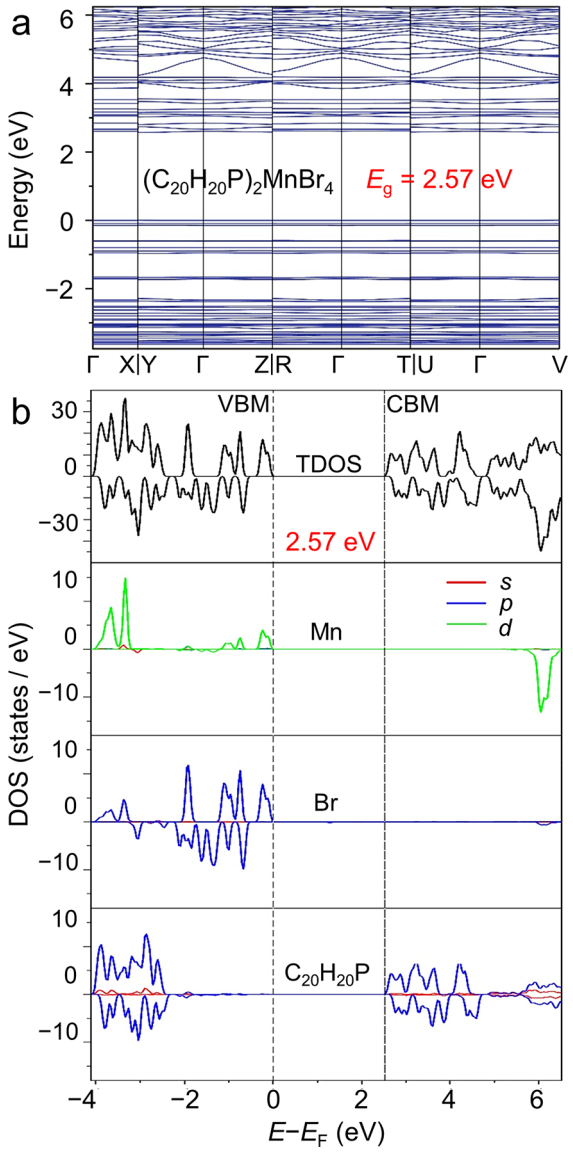

Figure 4. (a) Band structure of $(C_{20}H_{20}P)_2MnBr_4$ calculated with the high-accuracy HSE06 functional. (b) HSE06-calculated total and projected densities of states of $(C_{20}H_{20}P)_2MnBr_4$.

the temperature-dependent PL spectra of $(C_{20}H_{20}P)_2MnBr_4$ under excitation at 365 nm, and the inset is a variable trend of integrated intensity with the increase in temperature, illustrating that the intensities of the emission peaks gradually decrease as the temperature increases; at 100 °C, the variety is obvious and the PL-integrated intensity drops to 83.5% of the original intensity at 25 °C. The lifetimes of the PL decay for $(C_{20}H_{20}P)_2MnBr_4$ decrease gradually with the increase in temperature (Figure 3e), which is consistent with the variety trend of Figure 3d. Additionally, we consider that the weak interactions between $[C_{20}H_{20}P]^+$ and $[MnBr_4]^{2-}$ cause obvious lattice thermal vibration at higher temperatures, which enhances the lattice relaxation and the probability of nonradiative transitions, resulting in thermal quenching behavior. Figure 3f unravels the chemical stability of $(C_{20}H_{20}P)_2MnBr_4$ powder measured by employing thermogravimetric analysis (TGA) under a N_2 atmosphere, indicating that the compound has a good chemical stability without decomposition before 300 °C. Not only that, it was found that the emission intensity of $(C_{20}H_{20}P)_2MnBr_4$ synthesized a few months ago is almost not attenuated, which shows that it is very stable in the air. However, the emission intensity decreased significantly after aging for 120 h at 85% relative humidity (Figure S8), showing that $(C_{20}H_{20}P)_2MnBr_4$ is sensitive to water. To further evaluate its application prospect in solid-state displays, the LED devices were fabricated on the blue GaN chip (λ_{em} = 450 nm). Among them, the single-color LED device (LED-I) based on $(C_{20}H_{20}P)_2MnBr_4$ shows a high luminous efficacy of 177.65 lm/W. The white LED device (LED-II) is conducted by the green-emitting $(C_{20}H_{20}P)_2MnBr_4$, the red-emitting $K_2SiF_6:Mn^{4+}$, and the blue chip (λ_{em} = 450 nm). As shown in Figure 5a, the CIE

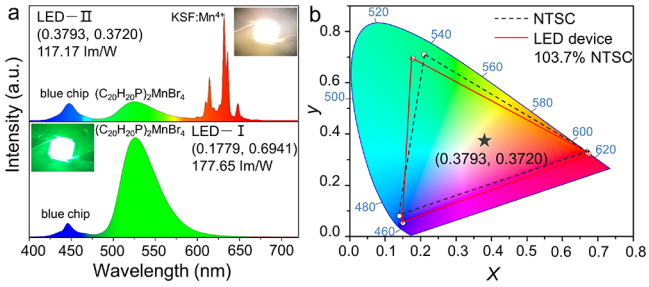

Figure 5. (a) PL spectra of white LED (LED-II) and green LED (LED-I). Insets show the photographs of the lightened LED devices. (b) Color gamut of the fabricated white LED device (red line, 103.7%) and the NTSC standard region (black dotted line) and the color coordinate of the fabricated white LED device (black star).

color coordinate of a white LED is (0.3793, 0.3720), the luminous efficacy is 117.17 lm/W, and the insets present the photographs of LED devices when the current is on. The current-dependent emission spectra from 20 to 300 mA change synchronously (Figure S9), and their CCT and CIE chromaticity coordinates have not changed significantly. Importantly, the color gamut of the as-fabricated white LED device is 103.7% NTSC standard compared with the standard value, as shown in Figure 5b, which demonstrates that $(C_{20}H_{20}P)_2MnBr_4$ is promising for display backlights.

CONCLUSIONS

In summary, a series of 0D Mn^{2+}-based halides with narrow-band green emissions can be prepared by continuous stirring in ethanol solution at RT for 5−10 s, and this in situ synthesis strategy of ultrafast self-assembly has been proposed and unraveled in essence. As a typical case, $(C_{20}H_{20}P)_2MnBr_4$ exhibits a bright and stable narrow-band green emission at 523 nm with an fwhm of 48 nm, which is attributed to the d−d transition ($^4T_1-^6A_1$) of tetrahedrally coordinated $[MnBr_4]^{2-}$ centers. The fabricated white LED presents a high luminous efficacy of 117.17 lm/W and a wide color gamut of 103.7% NTSC standard, indicating that these materials possess bright application prospects in solid-state displays. Remarkably, there are hydrogen bonding of C−H···Br and weak van der Waals interactions between $[C_{20}H_{20}P]^+$ and $[MnBr_4]^{2-}$ in $(C_{20}H_{20}P)_2MnBr_4$, resulting in the structural origin of ultrafast self-assembly. A brand-new synthesis strategy with the advantages of ultrafast self-assembly, easy operation, and low cost is reported for 0D Mn^{2+}-based halides. This work paves the way for the large-scale production of 0D Mn^{2+}-based halides in industrial applications.

https://doi.org/10.1021/acsaelm.1c00606
ACS Appl. Electron. Mater. 2021, 3, 4144−4150

■ ASSOCIATED CONTENT

Supporting Information

The Supporting Information is available free of charge at https://pubs.acs.org/doi/10.1021/acsaelm.1c00606.

Figure S1: crystal structure diagram and PLE/PL spectra of $(C_8H_8NS)_2MnBr_4$; Figure S2: CIE coordinates and digital; Figures S3 and S4: physical images and emission spectra and PL decay curves of single crystal, powder, and thin film; Figure S5: energy level of Mn^{2+} in a tetrahedral environment; Figure S6: PLQY calculation data; Figure S7: emission spectra and PL decay curves under different excitations; Figure S8: time-dependent PL spectra at an 85% humidity environment; Figure S9: emission spectra under different driving currents; Table S1: main bond lengths (Å); Table S2: fractional atomic coordinates and isotropic or equivalent isotropic displacement parameters (PDF)

Crystallographic data of $(C_{20}H_{20}P)_2MnBr_4$ (CIF)

Crystallographic data of $(C_8H_8NS)_2MnBr_4$ (CIF)

■ AUTHOR INFORMATION

Corresponding Authors

Jian Zhang − *Key Laboratory of Magnetic Molecules and Magnetic Information Materials (Ministry of Education), School of Chemistry and Material Science, Shanxi Normal University, Linfen 041004, China;* orcid.org/0000-0002-8089-9903; Email: zhangjian.net@yeah.net

Xian-Ming Zhang − *Key Laboratory of Magnetic Molecules and Magnetic Information Materials (Ministry of Education), School of Chemistry and Material Science, Shanxi Normal University, Linfen 041004, China; College of Chemistry & Chemical Engineering, Key Laboratory of Interface Science and Engineering in Advanced Material, Ministry of Education, Taiyuan University of Technology, Taiyuan, Shanxi 030024, P. R. China;* orcid.org/0000-0002-8809-3402; Email: zhangxm@dns.sxnu.edu.cn

Authors

Guojun Zhou − *Key Laboratory of Magnetic Molecules and Magnetic Information Materials (Ministry of Education), School of Chemistry and Material Science, Shanxi Normal University, Linfen 041004, China;* orcid.org/0000-0002-2450-3505

Qiqiong Ren − *Key Laboratory of Magnetic Molecules and Magnetic Information Materials (Ministry of Education), School of Chemistry and Material Science, Shanxi Normal University, Linfen 041004, China*

Maxim S. Molokeev − *Laboratory of Crystal Physics, Kirensky Institute of Physics, Federal Research Center KSC SB RAS, Krasnoyarsk 660036, Russia; Siberian Federal University, Krasnoyarsk 660041, Russia; Research and Development Department, Kemerovo State University, Kemerovo 650000, Russia;* orcid.org/0000-0002-8297-0945

Yayun Zhou − *State Key Laboratory of Luminescent Materials and Devices and Institute of Optical Communication Materials, South China University of Technology, Guangzhou 510641, China*

Complete contact information is available at: https://pubs.acs.org/10.1021/acsaelm.1c00606

Author Contributions

[▽]G.Z. and Q.R. contributed equally to this work.

Notes

The authors declare no competing financial interest.

■ ACKNOWLEDGMENTS

This work is supported by the Natural Science Foundation of China (no. 21871167) and the 1331 project of Shanxi Province and funded by RFBR according to the research project no. 19-52-80003.

■ REFERENCES

(1) Zhao, M.; Zhang, Q.; Xia, Z. Narrow-Band Emitters in LED Backlights for Liquid-Crystal Displays. *Mater. Today* **2020**, *40*, 246−265.

(2) Li, S. X.; Xie, R. J.; Takeda, T.; Hirosaki, N. Critical Review—Narrow-Band Nitride Phosphors for Wide Color-Gamut White LED Backlighting. *ECS J. Solid State Sci. Technol.* **2017**, *7*, R3064−R3078.

(3) Yan, C.; Lin, K.; Lu, J.; Wei, Z. Composition Engineering to Obtain Efficient Hybrid Perovskite Light-Emitting Diodes. *Front. Optoelectron.* **2020**, *13*, 282−290.

(4) Luo, B.; Li, F.; Xu, K.; Guo, Y.; Liu, Y.; Xia, Z.; Zhang, J. B-Site Doped Lead Halide Perovskites: Synthesis, Band Engineering, Photophysics, and Light Emission Applications. *J. Mater. Chem. C* **2019**, *7*, 2781−2808.

(5) Kahwagi, R. F.; Thornton, S. T.; Smith, B.; Koleilat, G. I. Dimensionality Engineering of Metal Halide Perovskites. *Front. Optoelectron.* **2020**, *13*, 196−224.

(6) Zhou, G.; Su, B.; Huang, J.; Zhang, Q.; Xia, Z. Broad-Band Emission in Metal Halide Perovskites: Mechanism, Materials, and Applications. *Mater. Sci. Eng. R: Rep.* **2020**, *141*, 100548.

(7) Zhou, C.; Lin, H.; Lee, S.; Chaaban, M.; Ma, B. Organic−Inorganic Metal Halide Hybrids beyond Perovskites. *Mater. Res. Lett.* **2018**, *6*, 552−569.

(8) Fu, P.; Hu, S.; Tang, J.; Xiao, Z. Material Exploration via Designing Spatial Arrangement of Octahedral Units: A Case Study of Lead Halide Perovskites. *Front. Optoelectron.* **2021**, 252.

(9) Morad, V.; Cherniukh, I.; Pöttschacher, L.; Shynkarenko, Y.; Yakunin, S.; Kovalenko, M. V. Manganese(II) in Tetrahedral Halide Environment: Factors Governing Bright Green Luminescence. *Chem. Mater.* **2019**, *31*, 10161−10169.

(10) Zhou, G.; Liu, Z.; Huang, J.; Molokeev, M.; Xiao, Z.; Ma, C.; Xia, Z. Unraveling the Near-Unity Narrow-Band Green Emission in Zero-Dimensional Mn^{2+}-Based Metal Halides: A Case Study of $(C_{10}H_{16}N)_2Zn_{1-x}MnxBr_4$ Solid Solutions. *J. Phys. Chem. Lett.* **2020**, *11*, 5956−5962.

(11) Zhou, G.; Liu, Z.; Molokeev, M.; Xiao, Z.; Xia, Z.; Zhang, X.-M. Manipulation of Cl/Br Transmutation in Zero-Dimensional Mn^{2+}-Based Metal Halides toward Tunable Photoluminescence and Thermal Quenching Behaviors. *J. Mater. Chem. C* **2021**, *9*, 2047−2053.

(12) Gong, L.-K.; Hu, Q.-Q.; Huang, F.-Q.; Zhang, Z.-Z.; Shen, N.-N.; Hu, B.; Song, Y.; Wang, Z.-P.; Du, K.-Z.; Huang, X.-Y. Efficient Modulation of Photoluminescence by Hydrogen Bonding Interactions between Inorganic $[MnBr_4]^{2-}$ Anions and Organic Cations. *Chem. Commun.* **2019**, *55*, 7303−7306.

(13) Li, S.; Wang, L.; Tang, D.; Cho, Y.; Liu, X.; Zhou, X.; Lu, L.; Zhang, L.; Takeda, T.; Hirosaki, N.; Xie, R.-J. Achieving High Quantum Efficiency Narrow-Band β-Sialon:Eu^{2+} Phosphors for High-Brightness LCD Backlights by Reducing the Eu^{3+} Luminescence Killer. *Chem. Mater.* **2018**, *30*, 494−505.

(14) Yuan, L.; Jin, Y.; Su, Y.; Wu, H.; Hu, Y.; Yang, S. Optically Stimulated Luminescence Phosphors: Principles, Applications, and Prospects. *Laser Photonics Rev.* **2020**, *14*, 2000123.

(15) Hong, K.; Le, Q. V.; Kim, S. Y.; Jang, H. W. Low-Dimensional Halide Perovskites: Review and Issues. *J. Mater. Chem. C* **2018**, *6*, 2189−2209.

(16) Sen, A.; Swain, D.; Guru Row, T. N.; Sundaresan, A. Unprecedented 30 K Hysteresis Across Switchable Dielectric and

Magnetic Properties in a Bright Luminescent Organic−Inorganic Halide $(CH_6N_3)_2MnCl_4$. *J. Mater. Chem. C* **2019**, *7*, 4838−4845.
(17) Zhang, Y.; Liao, W.-Q.; Fu, D.-W.; Ye, H.-Y.; Chen, Z.-N.; Xiong, R.-G. Highly Efficient Red-Light Emission in An Organic−Inorganic Hybrid Ferroelectric: (Pyrrolidinium)$MnCl_3$. *J. Am. Chem. Soc.* **2015**, *137*, 4928−4931.
(18) Wang, S.; Han, X.; Kou, T.; Zhou, Y.; Liang, Y.; Wu, Z.; Huang, J.; Chang, T.; Peng, C.; Wei, Q.; Zou, B. Lead-Free Mn^{II}-based Red-Emitting Hybrid Halide $(CH_6N_3)_2MnCl_4$ toward High Performance Warm WLEDs. *J. Mater. Chem. C* **2021**, *9*, 4895−4902.
(19) Su, B.; Molokeev, M.; Xia, Z. Mn^{2+}-Based Narrow-Band Green-Emitting Cs_3MnBr_5 Phosphor and the Performance Optimization by Zn^{2+} Alloying. *J. Mater. Chem. C* **2019**, *7*, 11220−11226.
(20) Peng, Y.; Li, L.; Ji, C.; Wu, Z.; Wang, S.; Liu, X.; Yao, Y.; Luo, J. Tailored Synthesis of an Unprecedented Pb−Mn Heterometallic Halide Hybrid with Enhanced Emission. *J. Am. Chem. Soc.* **2019**, *141*, 12197−12201.
(21) Song, P.; Qiao, B.; Song, D.; Cao, J.; Shen, Z.; Xu, Z.; Zhao, S.; Wageh, S.; Al-Ghamdi, A. Modifying the Crystal Field of $CsPbCl_3$:Mn^{2+} Nanocrystals by Co-doping to Enhance Its Red Emission by a Hundredfold. *ACS Appl. Mater. Interfaces* **2020**, *12*, 30711−30719.
(22) Zhou, C.; Tian, Y.; Khabou, O.; Worku, M.; Zhou, Y.; Hurley, J.; Lin, H.; Ma, B. Manganese-Doped One-Dimensional Organic Lead Bromide Perovskites with Bright White Emissions. *ACS Appl. Mater. Interfaces* **2017**, *9*, 40446−40451.
(23) Hu, G.; Xu, B.; Wang, A.; Guo, Y.; Wu, J.; Muhammad, F.; Meng, W.; Wang, C.; Sui, S.; Liu, Y.; Li, Y.; Zhang, Y.; Zhou, Y.; Deng, Z. Stable and Bright Pyridine Manganese Halides for Efficient White Light-Emitting Diodes. *Adv. Funct. Mater.* **2021**, *31*, 2011191.
(24) Zhang, S.; Zhao, Y.; Zhou, J.; Ming, H.; Wang, C.-H.; Jing, X.; Ye, S.; Zhang, Q. Structural DesignEnables Highly-Efficient Green Emission with Preferable Blue Light Excitation from Zero-Dimensional Manganese (II) Hybrids. *Chem. Eng. J.* **2021**, *421*, 129886.
(25) Mao, L.; Guo, P.; Wang, S.; Cheetham, A. K.; Seshadri, R. Design Principles for Enhancing Photoluminescence Quantum Yield in Hybrid Manganese Bromides. *J. Am. Chem. Soc.* **2020**, *142*, 13582−13589.
(26) Bai, X.; Zhong, H.; Chen, B.; Chen, C.; Han, J.; Zeng, R.; Zou, B. Pyridine-Modulated Mn Ion Emission Properties of $C_{10}H_{12}N_2MnBr_4$ and $C_5H_6NMnBr_3$ Single Crystals. *J. Phys. Chem. C* **2018**, *122*, 3130−3137.
(27) Li, M.; Zhou, J.; Molokeev, M.; Jiang, X.; Lin, Z.; Zhao, J.; Xia, Z. Lead-Free Hybrid Metal Halides with a Green-Emissive $[MnBr_4]$ Unit as a Selective Turn-On Fluorescent Sensor for Acetone. *Inorg. Chem.* **2019**, *58*, 13464−13470.
(28) Xu, L.; Gao, J. X.; Chen, X. G.; Hua, X. N.; Liao, W. Q. A Temperature-Triggered Triplex Bistable Switch in a Hybrid Multifunctional Material: $[(CH_2)_4N(CH_2)_4]_2[MnBr_4]$. *Dalton Trans.* **2018**, *47*, 16995−17003.
(29) Lu, T.; Chen, F. Multiwfn: A Multifunctional Wavefunction Analyzer. *J. Comput. Chem.* **2012**, *33*, 580−592.
(30) Hehre, W. J.; Ditchfield, R.; Pople, J. A. Self—Consistent Molecular Orbital Methods. XII. Further Extensions of Gaussian—Type Basis Sets for Use in Molecular Orbital Studies of Organic Molecules. *J. Chem. Phys.* **1972**, *56*, 2257−2261.
(31) Wadt, W. R.; Hay, P. J. Ab Initio Effective Core Potentials for Molecular Calculations. Potentials for Main Group Elements Na to Bi. *J. Chem. Phys.* **1985**, *82*, 284−298.
(32) Kresse, G. F. l. J.; Furthmüller, J. Efficient Iterative Schemes for Ab Initio Total-Energy Calculations Using a Plane-Wave Basis Set. *Phys. Rev. B* **1996**, *54*, 11169−11186.
(33) Perdew, J. P.; Burke, K.; Ernzerhof, M. Generalized Gradient Approximation Made Simple. *Phys. Rev. Lett.* **1996**, *77*, 3865−3868.
(34) Heyd, J.; Scuseria, G. E.; Ernzerhof, M. Hybrid Functionals Based on a Screened Coulomb Potential. *J. Chem. Phys.* **2003**, *118*, 8207−8215.
(35) Lefebvre, C.; Rubez, G.; Khartabil, H.; Boisson, J. C.; Contreras-Garcia, J.; Henon, E. Accurately Extracting the Signature of Intermolecular Interactions Present in the NCI Plot of the Reduced Density Gradient Versus Electron Density. *Phys. Chem. Chem. Phys.* **2017**, *19*, 17928−17936.
(36) Marenich, A. V.; Cramer, C. J.; Truhlar, D. G. Universal Solvation Model Based on Solute Electron Density and on a Continuum Model of the Solvent Defined by the Bulk Dielectric Constant and Atomic Surface Tensions. *J. Phys. Chem. B* **2009**, *113*, 6378−6396.
(37) Koscher, B. A.; Swabeck, J. K.; Bronstein, N. D.; Alivisatos, A. P. Essentially Trap-Free $CsPbBr_3$ Colloidal Nanocrystals by Postsynthetic Thiocyanate Surface Treatment. *J. Am. Chem. Soc.* **2017**, *139*, 6566−6569.

https://doi.org/10.1021/acsaelm.1c00606
ACS Appl. Electron. Mater. 2021, 3, 4144−4150